ELSEVIER

Results from new GPS and gravity monitoring networks at Fernandina and Sierra Negra Volcanoes, Galápagos, 2000–2002

Dennis Geist [a],[*],[1], William Chadwick [b],[1], Daniel Johnson [c],[1]

[a] *Department of Geological Sciences, University of Idaho-3022, Moscow, ID, 83844, USA*
[b] *Oregon State University/NOAA, 2115 SE OSU Drive, Newport, OR, 97365, USA*
[c] *Department of Earth and Space Sciences, University of Washington, Seattle, WA, 98195, USA*

Abstract

GPS and gravity networks were established on Sierra Negra and Fernandina volcanoes in 2000 and remeasured in 2001 and 2002. After a decade in which the caldera inflated by over 2.5 m, Sierra Negra's caldera began to subside between 2000 and 2002, at a rate of about 9 cm/a. Neither inflation nor deflation was accompanied by eruption. Simple elastic modeling indicates that the deformation at Sierra Negra can be attributed to volumetric contraction of a 2.1 km-deep sill beneath the caldera, caused by either movement of magma out of the sill or loss of bubbles through degassing. Precise gravity measurements support but do not prove the former mechanism. Fernandina volcano is in a phase of slow refilling of the summit reservoir after the 1995 eruption, causing lateral expansion of the caldera rim by about 3 cm/a. Our estimate for the depth of the shallowest part of the Fernandina magma chamber is 1 to 2 km. Neither volcano shows evidence of flank spreading.
© 2005 Elsevier B.V. All rights reserved.

Keywords: Galápagos Islands; calderas; magmas; geodesy; deformation

1. Introduction

Although the Galápagos volcanoes are some of the most active on Earth, they have been virtually unmonitored by geodetic methods until recently. This contrasts sharply with Hawaiian volcanoes, where deformation measurements have been conducted for most of the last century (Wilson, 1935; Dvorak and Dzurisin, 1997). Nevertheless, many important volcanological questions can be addressed by monitoring deformation on Galápagos volcanoes. For example, how and why calderas form on basaltic volcanoes remains enigmatic, and few basaltic volcanoes on the planet have calderas as voluminous and active as those in the Galápagos. Unlike their silicic counterparts, where collapse takes place in response to the catastrophic emptying of the magma reservoir during voluminous eruptions (e.g. Lipman, 1997), most basaltic calderas form by smaller and more frequent incremental events. In fact, one

* Corresponding author. Tel.: +1 208 885 6491.
  E-mail address: dgeist@uidaho.edu (D. Geist).
[1] The three authors contributed equally to this work.

hypothesis is that the formation of calderas at Hawaiian volcanoes is largely unrelated to eruption and instead is a response to the loading of dense ultramafic rocks beneath their summits (Walker, 1988).

The western Galápagos (Fig. 1) have some of the largest calderas of any basaltic volcanoes on the planet (Wood, 1984). Geologic evidence indicates that Galápagos calderas collapse in many phases, sometimes punctuated by partial refilling (e.g. Rowland and Munro, 1992; Geist et al., 1994; Naumann and Geist, 2000; Geist et al., 2002, 2003), major avalanching (Chadwick et al., 1991), and trapdoor uplift (Reynolds et al., 1995). The relationship between caldera formation and the underlying magmatic systems is unclear, however. For example, although the 1968 eruption of Fernandina resulted in about 300 m of caldera collapse, the volume of the collapse was over 100 times greater than the volume of lava erupted during the event (Simkin and Howard, 1970). On the other hand, the volume of the 1979 eruption of Sierra Negra was nearly 1 km^3, yet resulted in no major caldera collapse (Reynolds et al., 1995).

Another enigmatic characteristic of the western Galápagos shields is the orientation and distribution of fissure vents about the calderas. Most of the Galápagos shields have arcuate vents that are parallel to the caldera rims in their upper flanks, termed "circumferential fissures", and radial fissures on their lower flanks (Banfield et al., 1956; McBirney and Williams, 1969; Simkin, 1984). This unusual pattern of eruptive fissures is very distinct in the Galápagos and relatively rare elsewhere, but it is unclear why (Chadwick and Howard, 1991). The geometry of the fissures has been proposed to be due to a combination of slope stresses and upward pressure exerted by the shallow magma reservoirs (Chadwick and Dieterich, 1995). Alternatively, the same fissure pattern can be explained by contraction of the shallow reservoir or gravitational dragging by dense cumulates (Poland, 2001).
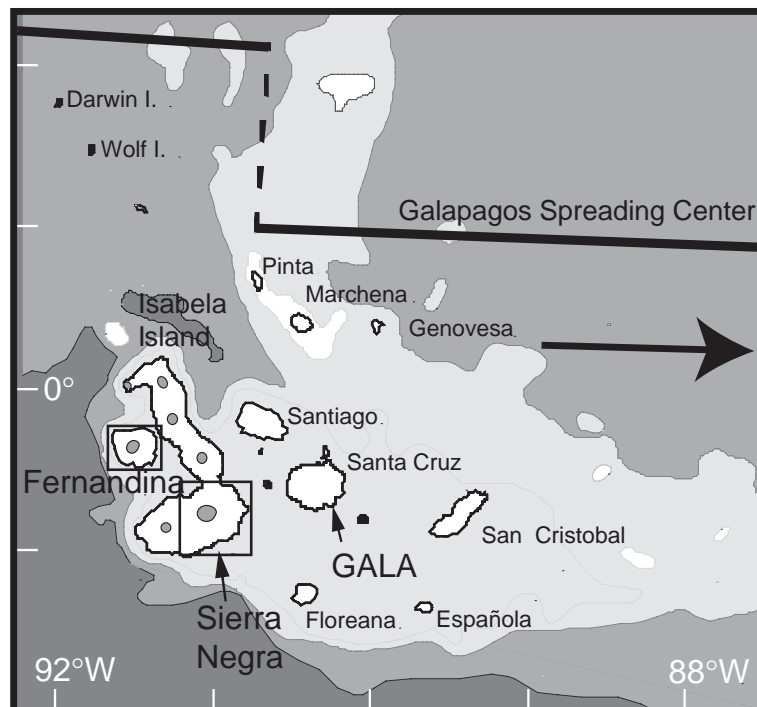

Fig. 1. The Galápagos Islands lie on the east-moving (large arrow, which indicates the absolute plate motion) Nazca Plate, immediately south of the Galápagos Spreading Center. The calderas of the seven large shields in the western archipelago are indicated in gray. The location of IGS station GALA is also shown. Boxes outline the study areas, Sierra Negra and Fernandina volcanoes.

Large-scale flank instability is a common phenomenon on ocean-island volcanoes (Moore et al., 1994; Lénat et al., 1989; Holcomb and Searle, 1991), and feedback between flank slip and rift zone extension is especially well-documented at Kilauea (Swanson et al., 1976; Dieterich, 1988; Owen et al., 1995). It is unclear how important a process this is in the Galápagos, however. Prehistoric large-scale mass wasting has been documented on Pinta (Cullen et al., 1987), Cerro Azul (Naumann and Geist, 2000), and Ecuador volcanoes (Geist et al., 2002), but no active flank landslides have been recognized in the Galápagos.

In order to clarify the relationship between magma movement and the growth and evolution of Galápagos shield volcanoes and to test the various hypotheses proposed above, we installed new GPS and gravity monitoring networks at Sierra Negra and Fernandina volcanoes (Figs. 2 and 3). These networks are the first systematic, ground-based deformation measurements on Galápagos volcanoes. Three GPS and gravity campaigns were performed in January 2000, January 2001, and May–June 2002 to constrain the three-dimensional deformational field. No eruptive activity occurred during this time inter-
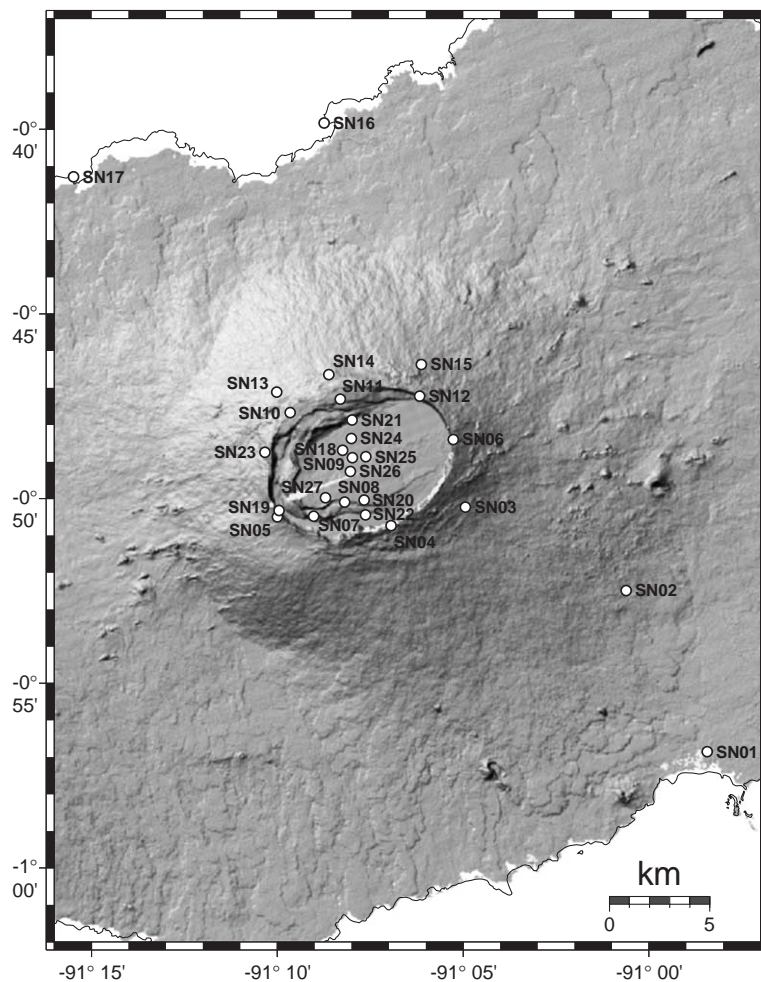

Fig. 2. The Sierra Negra network comprises 26 stations, most around and within the caldera. Digital elevation model in all figures is from TOPSAR experiment and kindly provided by Peter Mouginis-Mark and georeferenced by Chris Small and Dan Scheirer. Blank areas in topography in all further figures were not covered by the TOPSAR data.
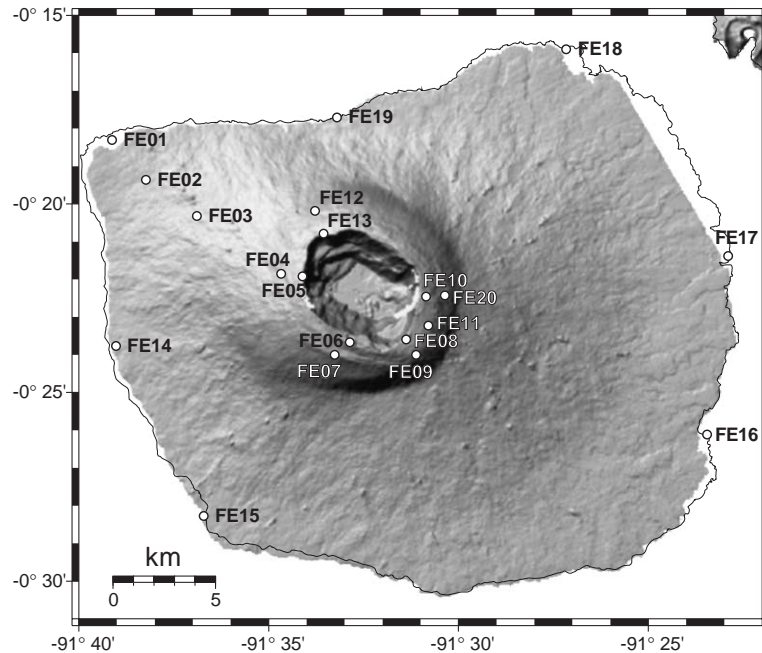
Fig. 3. The Fernandina GPS network comprises 20 stations.

val: Sierra Negra last erupted in 1979 and Fernandina in 1995.

2. Geologic background

The Galápagos islands are related to a hotspot adjacent to a mid-ocean ridge (Fig. 1). The islands lie on the Nazca plate, whose absolute motion is eastward; thus, the youngest volcanoes are in the western part of the archipelago. The western Galápagos volcanoes are dominantly basaltic and constituted of differentiated tholeiitic basalt. The western Galápagos is the type locality for the "Galápagos Shield" morphologic type of shield volcano (Williams and McBirney, 1979), which are characterized by their steep upper flanks, proportionately large calderas, arcuate summit fissures, and radial flank fissures.

Fernandina is the most active volcano in the archipelago, having experienced 23 observed eruptions since 1813 (Simkin and Siebert, 1994). Its most recent eruption was in 1995, which vented from a radial rift on the southwest flank of the volcano. Fernandina is perhaps best known for the major caldera collapse that occurred in 1968 (Simkin and Howard, 1970).

Although Sierra Negra is the lowest-lying of the western Galápagos shields and has the shallowest caldera, it is the most voluminous, and it has had 11 observed eruptions. The most recent of these was in 1979, when nearly the entire northern flank was covered by lava erupted from a circumferential fissure.

3. Previous deformation studies

No long-term, in situ deformation monitoring has previously been carried out in the Galápagos. In the 1990's, satellite radar interferometry (InSAR) studies indicated that the caldera floor of Sierra Negra Volcano inflated by about 2.5 m between 1992 and 1999, at rates as high as 60 cm/a (Amelung et al., 2000). From 1992 to 1997, the center of uplift was near the center of the caldera. From late 1997 through 1998, uplift was instead centered on the southern segment of the U-shaped sinuous fault system which borders a tilted horst that occupies the western half of the caldera (Fig. 2; Amelung et al., 2000; Reynolds et al., 1995). This was interpreted as being due to 1.2 m of uplift along a trapdoor fault, which culminated 5 yrs of inflation of a 1.9 km-deep sill (Amelung et al.,

2000). Between 1998 and 1999, the center of uplift shifted back to the center of the caldera.

The InSAR results at Fernandina are dominated by the effects of the 1995 eruption, which produced a semi-circular shaped deformation pattern about the 1995 radial eruptive fissure, interpreted as swelling above a dipping dike on the southwest flank of the volcano (Jonsson et al., 1999).

Previous GPS measurements in Galápagos have only been made as part of regional tectonic networks. The Galápagos islands are one of the few places from which the motion of the Nazca Plate can be directly measured. The CASA GPS network was installed in 1991 and extends over northwestern South America (Freymueller et al., 1993). CASA includes one GPS station in Galápagos on the island of Baltra that has been occupied during periodic campaigns. The continuously recording GALA IGS (International GPS Service) site on Santa Cruz island was installed in 1996 and replaced in 2003 by GLPS.

Satellite-based InSAR and ground-based GPS are both effective methods for measuring volcanic deformation, but there are some key differences in the information provided by each technique. InSAR can quantify deformation over large continuous areas, whereas GPS only measures displacement from established monitoring points. On the other hand, GPS yields three components of motion for each station (two horizontal and one vertical), whereas InSAR only yields one range change along the look direction from the satellite (which is usually inclined from vertical). In addition, the frequency of InSAR measurements is constrained by the timing of satellite orbits, whereas GPS measurements depend on field schedules (campaign) or can be continuous.

4. Methods

The GPS measurements reported here were made over the course of 3 yrs. The networks were designed to capture movement of the caldera floor on Sierra Negra (the caldera floor of Fernandina is virtually inaccessible), to capture displacements due to dike emplacement from either circumferential or radial fissures, and to measure potential flank slip. Most stations are monumented with a brass cap that has been cemented into a hole drilled into bedrock. Where

no bedrock was available, stations consist of steel construction rods ("rebar") driven to refusal. All sites are described and documented at http://www.webpages.uidaho.edu/~dgeist/GPS/G4.html.

The 2000 campaign took place between January 2–9 on Sierra Negra and January 11–20 on Fernandina. Leica SR9500 receivers were used with a choke-ring antenna fixed on tri-bracketed tripods with optical plumbs. The 2001 and 2002 campaigns used Trimble 4700 and 4000 SSI receivers with choke-ring antennas. Some of the antennas were mounted on fixed-height tripods. The 2001 Sierra Negra campaign was January 5–13, and the Fernandina campaign was from January 16 to 24. Prior to the switch from Leica to Trimble receivers, a control experiment was performed in Ellensburg, WA, USA using two fixed antennas and switching the receivers. The two brands of receivers gave processed results that were identical within 3 mm in all three directions. The 2002 Sierra Negra campaign was between May 24 and June 3 and the Fernandina campaign June 4 and 13. The minimum measuring interval was 14 h, although most stations were monitored for >24 h. Six stations were usually measured simultaneously in each campaign.

GPS data were processed using Bernese 4.2 software (Hugentobler et al., 2001), with baselines processed using precise orbit and pole determinations from the IGS. The data were processed with cycle slips removed, tropospheric corrections, ambiguity resolution, and network solutions.

During the 2000 campaign, the only continuously-recording instrument in the region (GALA) was not operating. Instead, in 2000, SN01 was monitored for the entire campaign (8 days) at Sierra Negra (Fig. 2), and FE01 was monitored during the entire campaign at Fernandina (Fig. 3). Their positions were then determined using >1000 km baselines with the RIOP, AREQ, and EISL IGS stations constrained to their ITRF2000 positions. The other stations' positions on both Sierra Negra and Fernandina in 2000 were then calculated in reference to those determined positions. The 2001 and 2002 positions are relative to GALA, constrained to its ITRF2000 reference frame coordinates. GALA is roughly 100 km from the local networks (Fig. 1). Velocities are calculated relative to GALA for the 2001 and 2002 campaigns at both volcanoes. The 2000–2001 velocities are calculated by fixing SN05, SN06, and SN14, which all lie on the

Table 1
GPS measured velocities

	Bernese						Gipsy								
	North	±	East	±	Vertical	±	North	East	Vertical	North	East	Vertical	North	East	Vertical
Station 2000–2001										Difference			(Residuals - Offsets)		
SN01	−1.7	2.0	−5.1	2.4	−34.7	9.9	2	−9	−1	−4.2	4.0	−33.5	−8.7	−5.7	−34.4
SN04	16.1	2.8	−3.8	3.5	8.3	14.5				16.1	−3.8	8.3			
SN05	0.0		0.0		0.0		−9	−8	−1	9.0	8.0	0.9	4.5	−1.6	0.0
SN06	0.0		0.0		0.0		−3	−19	11	2.9	18.5	−11.5	−1.6	8.8	−12.4
SN07	18.2	2.2	1.3	3.1	−9.8	13.5	13	−12	−8	4.9	13.7	−2.1	0.3	4.0	−3.0
SN08	3.9	2.1	0.3	2.7	−17.9	12.0	9	−11	−4	−4.9	11.0	−13.5	−9.4	1.4	−14.4
SN09	7.8	2.2	7.0	3.1	67.9	13.5	−1	−11	70	9.3	18.3	−2.4	4.7	8.6	−3.3
SN11	2.8	2.1	5.0	2.8	−8.7	12.1	0	−1	−4	3.2	6.3	−4.8	−1.3	−3.4	−5.7
SN12	6.1	1.5	20.4	2.0	−14.2	9.1	7	12	11	−1.0	8.5	−25.4	−5.5	−1.2	−26.3
SN14	0.0		0.0		0.0		2	−3	−5	−1.8	2.8	5.3	−6.3	−6.9	4.4
SN15	2.3	2.8	−9.9	3.1	−5.0	13.4				2.3	−9.9	−5.0			
SN19	8.4	2.1	−6.7	2.8	−11.3	12.0				8.4	−6.7	−11.3			
SN21	−4.0	3.1	2.2	4.5	−22.8	17.9	−3	−10	−18	−0.9	12.4	−4.9	−5.4	2.7	−5.8
SN23	13.8	2.7	3.7	3.5	−17.8	15.8	19	−16	1	−5.6	19.6	−19.2	−10.1	9.9	−20.1
FE01	−26.8	1.3	−1.8	1.8	−0.2	6.9	−33	−7	−9	6.6	5.0	8.9	2.1	−4.7	8.0
FE02	−11.5	2.1	6.6	2.9	−0.2	13.4	−20	−2	−10	8.8	9.0	9.6	4.3	−0.7	8.7
FE03	20.5	2.1	3.9	2.9	3.1	13.2	9	6	−4	11.7	−2.0	6.9	7.2	−11.6	5.9
FE04	4.0	2.2	−9.7	2.9	−7.7	13.4	−4	−12	2	8.4	2.5	−9.5	3.9	−7.2	−10.4
FE06	−22.3	2.4	−2.6	3.1	4.7	12.0	−29	−22	2	6.7	19.4	3.2	2.2	9.8	2.3
FE07	−19.5	2.4	−9.7	2.8	−10.5	11.5	−23	−26	−7	3.4	16.2	−3.8	−1.2	6.6	−4.8
FE09	−2.8	1.7	0.0	2.5	−9.2	10.2	−10	−5	−7	7.1	4.8	−2.3	2.6	−4.8	−3.2
FE12	11.7	2.1	−5.8	2.8	8.5	12.9	−1	−13	−20	12.4	7.3	28.7	7.8	−2.3	27.8
FE13	10.0	2.1	−7.1	3.1	13.0	12.2	3	−22	−7	6.8	15.4	20.3	2.3	5.7	19.4
FE15							−17	−9	−18	17.0	8.8	17.9	12.5	−0.9	17.0
FE16							9	0	−27	−8.9	0.3	27.4	−13.4	−9.4	26.4
FE17							−6	−10	−27	5.7	10.0	26.7	1.1	0.3	25.8
FE18							−12	−12	1	12.1	12.2	−0.9	7.5	2.5	−1.8
									Average	4.5	9.7	0.9	0.2	−0.1	0.0
Station 2001–2002										Difference			(Residuals - Offsets)		
GALA	0		0		0		16.1	−14.5	1.1	−16.1	14.5	−1.1	−0.2	−1.4	−14.0
SN01	8	1.4	11	2.1	16	8.6	20.9	−14.7	−16.4	−13.3	25.5	32.8	2.7	9.5	20.0
SN02	−6	1.8	6	2.5	−11	10.5	13.6	−11.4	1.7	−19.4	17.2	−13.1	−3.5	1.3	−26.0
SN03	10	1.4	1	2.0	1	9.3	21.4	−13.3	−11.4	−11.5	14.7	12.0	4.4	−1.3	−0.8
SN04	15	1.7	−1	2.2	9	10.3	44.7	−24.1	−14.5	−30.0	23.0	23.3	−14.1	7.1	10.5
SN05	7	1.4	18	1.4	2	9.4	26.8	2.0	−10.3	−19.6	16.3	12.0	−3.7	0.3	−0.9
SN06	−1	1.3	−9	1.8	−5	8.1	9.7	−24.0	−19.7	−10.7	14.7	14.9	5.2	−1.3	2.1
SN07	23	1.4	14	2.0	−5	8.6	38.8	−1.3	−30.4	−15.9	15.0	25.8	0.0	−1.0	12.9
SN08	51	1.3	2	1.7	−42	7.6	65.1	−16.8	−66.5	−14.1	18.4	24.8	1.8	2.4	12.0
SN09	−20	1.4	18	2.0	−89	8.6	3.0	2.0	−115.6	−22.6	16.3	26.1	−6.6	0.4	13.3
SN10	−17	1.3	18	1.7	−5	7.8	−1.9	1.5	−19.3	−15.6	16.3	14.7	0.3	0.4	1.9
SN11	−27	1.3	11	2.0	−7	8.1	−5.8	−4.5	−22.4	−21.3	15.1	15.5	−5.4	−0.9	2.7
SN12	−15	0.6	−17	0.8	3	3.4	1.1	−35.2	−24.4	−16.1	17.8	27.0	−0.2	1.8	14.1
SN13	−6	1.0	14	1.4	11	6.0	5.9	−4.7	−12.7	−12.0	19.0	23.9	3.9	3.1	11.0
SN14	−11	1.4	5	2.0	0	8.6	4.3	−12.1	−15.9	−15.3	16.9	15.5	0.7	1.0	2.7
SN15	−8	1.3	10	1.8	−69	7.8	8.2	−7.6	−14.5	−16.4	17.8	−54.7	−0.4	1.9	−67.6
SN16	0	1.5	8	2.1	−12	8.7	15.3	−18.6	−26.7	−15.4	27.0	15.0	0.5	11.0	2.1
SN17	0	1.4	6	2.2	−5	9.6	11.3	−13.5	−24.2	−10.9	19.9	19.3	5.0	3.9	6.5
SN18	−26	1.0	28	1.4	−83	6.1	−11.4	10.3	−100.4	−14.7	18.0	17.8	1.2	2.1	5.0

Table 1 (*contiued*)

	Bernese						Gipsy								
	North	±	East	±	Vertical	±	North	East	Vertical	North	East	Vertical	North	East	Vertical
Station 2001–2002										Difference			(Residuals - Offsets)		
SN19	12	1.5	20	2.2	1	9.9	32.6	0.8	−25.3	−20.8	19.3	26.1	−4.9	3.4	13.2
SN20	52	1.1	−7	1.4	−36	6.7	62.1	−23.6	−62.8	−10.0	16.1	26.9	6.0	0.2	14.0
SN21	−44	1.1	15	1.5	−36	7.2	−24.9	−2.9	−58.5	−19.2	18.1	22.1	−3.2	2.2	9.2
SN23	0	1.4	17	1.8	4	8.6	11.8	5.9	−12.0	−12.0	11.2	16.4	3.9	−4.8	3.6
SN24	−42	1.5	21	2.0	−59	9.4	−28.1	2.1	−92.0	−14.0	18.6	32.9	2.0	2.7	20.0
SN25	−9	1.1	−3	1.5	−90	7.1	3.3	−20.4	−111.8	−12.2	17.6	21.9	3.7	1.6	9.0
SN26	6	1.0	12	1.4	−95	6.2	17.0	−6.2	−111.0	−11.2	17.9	15.9	4.7	2.0	3.0
SN27	40	1.4	10	2.0	−59	8.9	59.6	−8.9	−57.5	−19.4	18.4	−1.8	−3.5	2.4	−14.7
FE01	15	0.6	−5	0.8	−16	3.3	30.7	−21.5	−7.7	−15.8	16.2	−7.9	0.1	0.2	−20.8
FE02	−7	1.4	5	1.8	0	8.9	10.9	−11.4	4.3	−17.9	16.9	−4.2	−2.0	1.0	−17.1
FE03	−4	1.4	−1	1.8	1	8.4	14.5	−25.0	−6.5	−18.7	24.0	7.3	−2.8	8.1	−5.5
FE04	−5	1.4	−3	2.1	−44	9.4	10.4	−21.8	−11.4	−15.5	18.5	−32.2	0.4	2.5	−45.0
FE05	0	1.4	2	2.0	22	8.9	17.4	−12.6	2.6	−17.7	14.5	19.0	−1.8	−1.5	6.2
FE06	−22	1.4	2	2.0	21	8.5	−0.4	−13.1	−9.3	−21.9	15.2	30.7	−5.9	−0.8	17.8
FE07	−16	1.0	0	1.4	22	6.3	6.1	−15.3	0.7	−22.2	15.4	20.9	−6.3	−0.6	8.1
FE08	−7	1.8	5	2.5	7	11.4	8.9	−12.1	−10.8	−16.1	17.3	17.8	−0.2	1.3	5.0
FE09	−7	1.0	6	1.4	7	6.2	7.9	−11.3	−1.7	−14.8	16.8	8.5	1.1	0.9	−4.4
FE10	−5	0.8	12	1.3	3	5.5	12.5	−3.5	−4.8	−17.3	15.6	7.6	−1.4	−0.3	−5.2
FE12	3	1.4	−1	2.0	−35	9.1	19.3	−15.4	−13.1	−16.5	14.5	−22.3	−0.6	−1.5	−35.2
FE13	4	1.5	6	2.1	−29	9.5	25.7	−11.7	−3.8	−21.6	18.0	−25.2	−5.6	2.0	−38.1
FE14	−2	1.5	3	2.1	21	9.4	14.3	−20.2	−12.9	−16.5	23.7	33.5	−0.6	7.7	20.6
FE15	0	2.4	5	2.1	14	9.5	17.0	−14.0	−6.5	−16.8	19.2	20.5	−0.9	3.2	7.6
FE16	−11	1.4	6	2.0	14	9.1	7.5	−6.4	−7.6	−18.4	12.0	21.7	−2.5	−4.0	8.8
FE17	−2	1.4	7	1.8	1	8.4	17.6	−10.0	−11.3	−19.9	17.2	12.1	−4.0	1.2	−0.7
FE18	−3	1.3	4	1.8	10	7.9	18.9	−6.8	−17.3	−21.7	11.0	27.6	−5.7	−4.9	14.7
FE19	−8	2.0	8	2.9	28	11.6	17.4	12.7	−15.1	−25.8	−4.5	42.7	−9.9	−20.4	29.8
FE20	−6	1.4	11	2.0	1	8.9	9.1	−9.0	−13.3	−15.3	19.8	13.9	0.6	3.9	1.1
DA01	−3	2.0	6	2.5	−20	12.2									
AL01	−3	2.0	5	2.9	−2	11.5									
									Average	−15.9	16.0	12.9	−1.0	1.0	0.3
Standard deviation:													5.0	5.2	17.7
1-sigma variation of single method compared to the other:													2.25	2.27	4.20

First three columns are as processed using Bernese 4.2 software and second three columns using Gipsy software. The differences and residuals with block offsets subtracted are also tabulated.

upper flanks of Sierra Negra and encompass most of the summit stations, and FE15, FE16, FE17, and FE18, which lie on the coast of Fernandina (Figs. 2 and 3, Table 1).

Uncertainties in velocity as reported by Bernese are unrealistically small. In this work, velocity precision is estimated by calculating the standard deviation of positions of stations that were measured for three or more days in each campaign. The position uncertainty is then propagated to velocity, and this velocity uncertainty divided by the individual stations' uncertainties reported by Bernese and averaged to calculate a scaling factor. These scaling factors are then multiplied by

each station's Bernese-reported uncertainty to obtain estimated velocity uncertainties (Table 1).

As a check on the Bernese results, GPS data were also processed using the GIPSY OASIS II software. The GIPSY processing was done in point-positioning mode using precise orbits and clock corrections provided by the Jet Propulsion Laboratory and has ambiguity resolution applied. At least eight IGS sites located within 3000 km were processed in combination with the Galápagos data so that the solution could be given in an ITRF2000 reference frame. Finally, the effects of motion of the Nazca plate were removed using the NNR NUVEL1 model. To first order, the

Bernese and GIPSY results agree well. A comparison of the solutions yields common-mode offsets of 5 to 15 mm. These uniform offsets are likely due to different choices of reference stations and the uncertainty of the reference station motions, especially for the 2000 campaign. When the average "block" motion is subtracted from the respective analysis and the annual motions are compared on a station by station basis, the average discrepancy suggests that the choice of analysis technique contributes only ± 2.2 mm to the 1-sigma variation in the horizontal component and ± 4.2 mm in vertical. Thus, the choice of processing software contributes little to the total error estimate.

Precise gravimetric observations were made in conjunction with the GPS campaigns to provide information on subsurface mass change. Two different LaCoste and Romberg model G gravimeters were used for each survey; one instrument was replaced in 2002. Each gravity survey was completed in 4 to 8 days, with each site revisited on at least two different days. Instrumental drift and relative gravity values were estimated simultaneously by a least-squares procedure that utilizes gravity readings from both gravimeters and from all the days of the survey (Johnson, 1992, 1995). Due to the long distances between sites which limited the number of readings that could be accomplished in a given day, only a linear instrumental drift model could be supported by the observations.

Estimates of the errors in the gravity solutions were provided by the covariance matrix which was scaled by the post-fit gravity observation residuals. Stations with the typical four independent gravity readings have standard errors estimated at ± 15 to 20 micro-gals. Very large errors are estimated for Fernandina flank sites (FE01, FE02, FE03, and FE04) where logistical considerations (1500 m of elevation change) precluded the normal practice of "closing" loops on the same day. Circular errors are not accounted for here due to difficulty in determining appropriate values. Circular errors are probably present in the gravimeters utilized. The impact of not including a circular error correction in the gravimeter calibrations would be greatest for the 2001–2002 interval, where one of the two gravimeters used was exchanged.

5. Results

5.1. Sierra Negra

The clearest deformational signal at Sierra Negra between 2000 and 2001 is vertical uplift of the center of the caldera (station SN09) by about 7 cm (Fig. 4). Otherwise, vertical velocities are less than measurement uncertainty with three exceptions. First, station SN01, which is near the south coast of Sierra Negra,
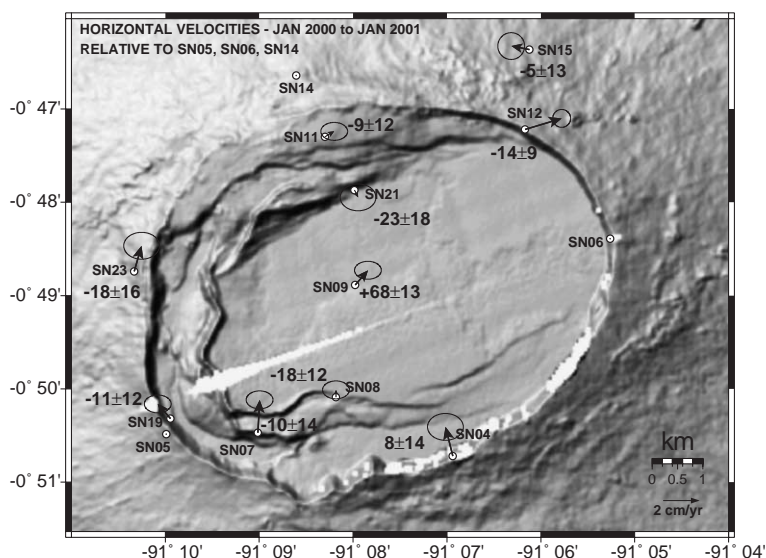

Fig. 4. Velocities (mm/a) of stations on the summit of Sierra Negra from January, 2000 to January, 2001.
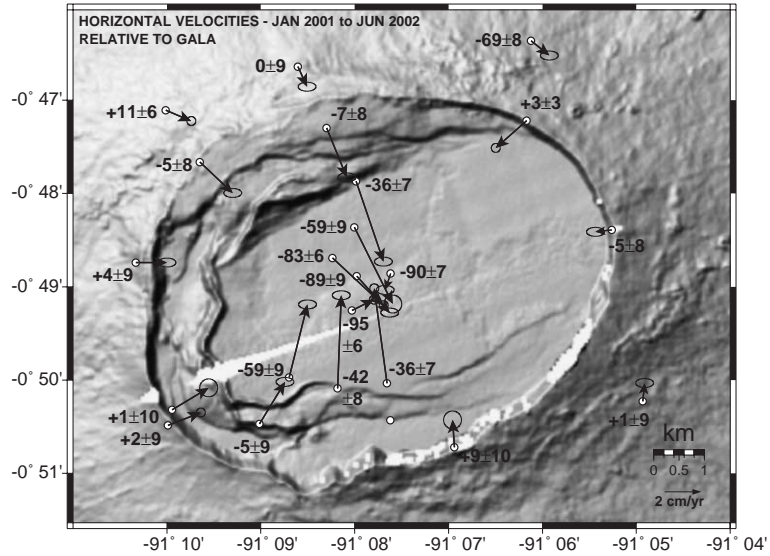
Fig. 5. Velocities of stations on the summit of Sierra Negra from January, 2001 to May, 2002.

shows a subsidence of 3.5 cm. Because this pattern does not continue into the 2001–2002 time interval (see below), we attribute this apparent subsidence to measurement error. Alternatively, it is conceivable that SN01 was actually stable and the entire summit region was uplifted by about 3 cm during 2000–2001 (recall that the 2000–2001 velocities at Sierra Negra are calculated relative to three stations near the summit). The second exception is that the station at the north end of the caldera floor, SN21, shows a down-
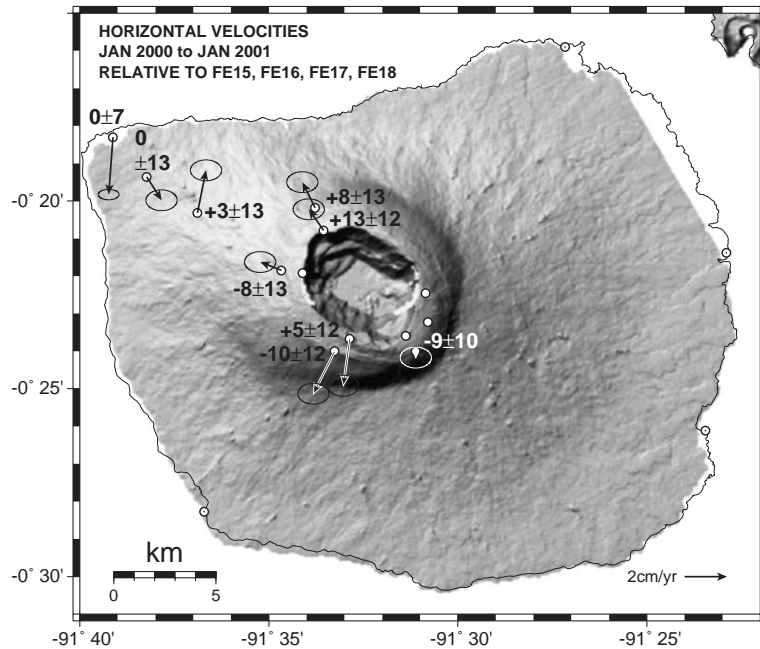

Fig. 6. Velocities of stations on the summit of Fernandina volcano from January, 2000 to January, 2001.

ward motion of 2.3 cm/a, which is greater than the estimated uncertainty. Third, SN08, located at the south margin of the caldera floor, shows a downward velocity of 1.7 cm/a. The symmetry of these motions about the center of the caldera suggests that the measurements may be real. The relatively low rate of uplift of the center of Sierra Negra's caldera is in marked contrast to the high rates of uplift measured by InSAR in the 1990s (Amelung et al., 2000), and the subsidence of the north and south parts of the caldera floor clearly indicate the start of a new deformational episode. The horizontal velocities in 2000–2001 are either less than the uncertainty or show no consistent pattern (Fig. 4).

The velocities measured between 2001 and 2002 reveal that the deformation of Sierra Negra's caldera floor changed from uplift to subsidence over the entire

summit region beginning in 2000 or 2001 (Fig. 5). The subsidence is greatest in the center of the caldera, where it amounts to 9 cm/a at stations SN09, SN25, and SN26. The subsidence decreases with radial distance from the center of the caldera, and the caldera rim stations display no significant vertical motions (Fig. 5). The more accurate horizontal velocities confirm the vertical measurements. All of the summit stations show significant horizontal motions, all moving towards the center of the caldera (Fig. 5). The distance between the north and south parts of the caldera floor (SN21 and SN08) decreased by 9.5 cm over the 17 month period.

Two stations positioned on the north coast of Sierra Negra (SN16 and SN17) measured no significant displacements (Table 1). In summary, after a decade of extraordinary uplift rates at Sierra Negra caldera,
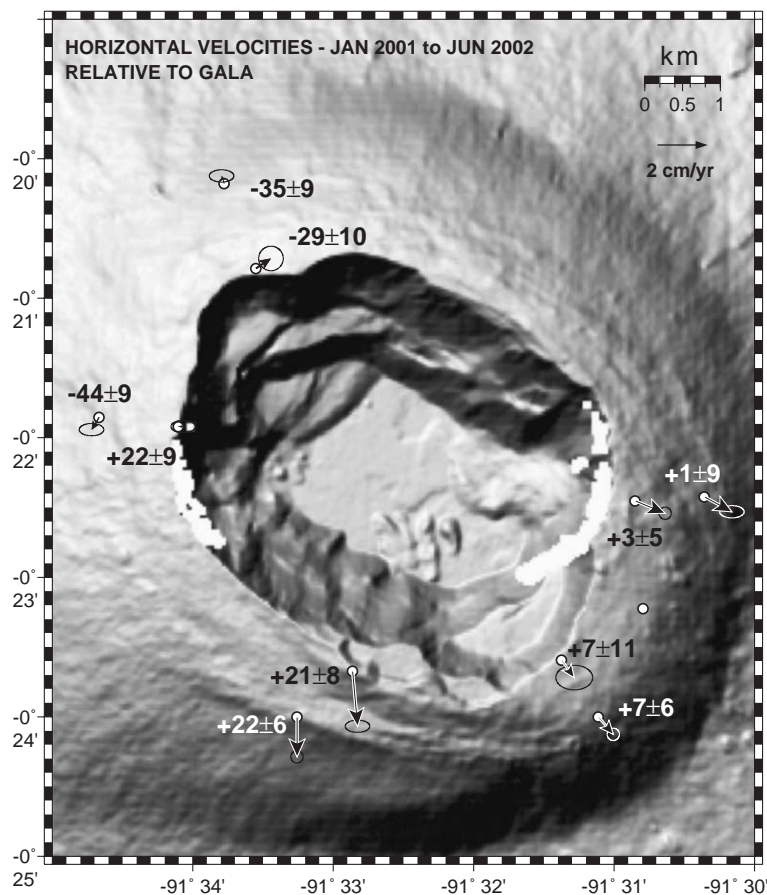

Fig. 7. Velocities of stations on the summit of Fernandina volcano from January, 2001 to May, 2002.

our GPS network captured the abrupt slowing of those rates (2000–2001) and the transition to caldera subsidence (2001–2002).

5.2. Fernandina

Between 2000 and 2001, the pattern of deformation at Fernandina was dominated by small radial-outward motions around the caldera rim (Fig. 6). The motions were asymmetrical, with the south rim (FE06 and FE07) moving outward at about 2 cm/a, and the north (FE12 and FE13) and west (FE04) rims moving outward at only about 1 cm/a. This pattern continued in the 2001–2002 interval, when the south caldera rim continued its southward motion at 2 cm/yr (Fig. 6). The north and west rims slowed to <1 cm/a, although those stations continued to move outward in a radial direction. Reliable baselines were also established for stations on the southeastern and eastern caldera rims in 2001–2002, and they also moved outward at about 1 cm/a. Therefore, horizontal extension across the caldera of ~3 cm/a is clearly resolved, consistent with inflation centered within the caldera. Vertical motions in 2000–2001 and 2001–2002 are barely greater than measurement uncertainty (Figs. 6 and 7). The southern and western caldera rims uplifted about 2 cm (FE05, FE06, and FE07), and the northern caldera rim dropped by about 3 cm (FE12 and FE13).

The coastal stations at Fernandina show no consistent motions over the duration of the study, and most measured horizontal velocities are <1 cm/a. Intriguingly, they have measured vertical velocities that average 1.5 cm/a upward. Because these velocities are relative to a station on Santa Cruz Island, this vertical motion may be attributable to either uplift of the entire Fernandina edifice, or subsidence of Santa Cruz island.

Station FE01 showed 2.7 cm of southward displacement in 2000–2001 and 1.5 cm of northward displacement in 2001–2002 (Fig. 8). This station was monitored continuously for the entire Fernandina campaign each year, to use as a fiducial site in the event of failure of GALA. Thus, its positions should be most accurate. There are no recent eruptive vents, faults, or other signs of deformation in the area. One possibility is that the antenna was disrupted or poorly positioned in 2001, as the net motion between 2000 and 2002 is small. Future campaigns may clarify whether these apparent motions were spurious or part of longer-term trends.
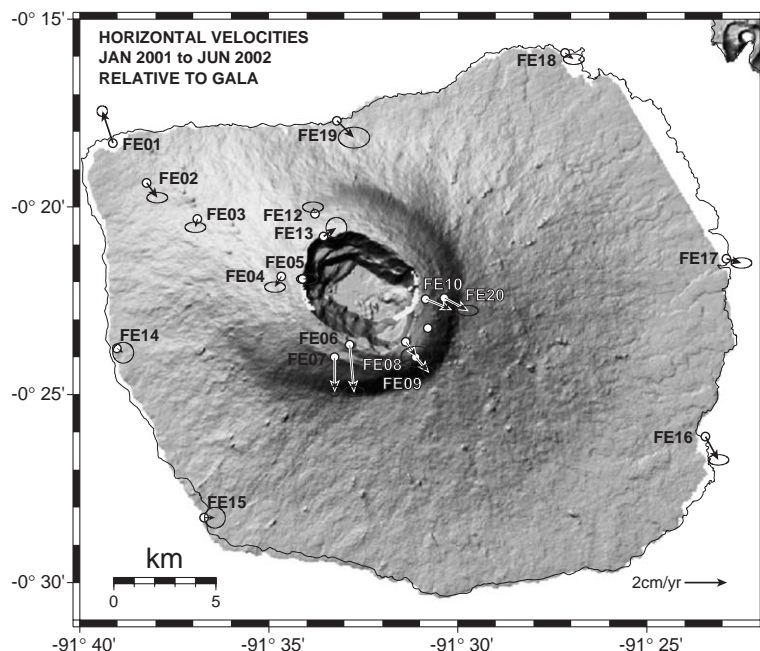

Fig. 8. 2001–2002 horizontal velocities around the coast of Fernandina.

Table 2
Reduced gravity changes at Fernandina and Sierra Negra Volcanoes

Station	2000	2001	2002	2000–2001	2001–2002
FE01	286.2457 ± 1.1484	286.7255 ± 0.1683	286.6878 ± 0.0445	0.4798 ± 1.1607	− 0.0377 ± 0.1741
FE02	280.4455 ± 0.9117	280.8115 ± 0.1300	280.8078 ± 0.0386	0.3660 ± 0.9210	− 0.0037 ± 0.1356
FE03	219.0517 ± 0.6799	219.3139 ± 0.0927	219.3131 ± 0.0326	0.2622 ± 0.6862	− 0.0008 ± 0.0983
FE3A	160.3635 ± 0.4793	160.5368 ± 0.0585	160.5649 ± 0.0253	0.1733 ± 0.4828	0.0281 ± 0.0637
FE04	49.0761 ± 0.1923	49.1331 ± 0.0180	49.1373 ± 0.0162	0.057 ± 0.1931	0.0042 ± 0.0242
FE05	0 ± 0.0000	0 ± 0.0000	0 ± 0.0000	0 ± 0.0000	0 ± 0.0000
FE06	− 10.4995 ± 0.0188	− 10.5408 ± 0.0117	− 10.5392 ± 0.0125	− 0.0413 ± 0.0221	0.0016 ± 0.0171
FE07	15.1025 ± 0.0194	15.0693 ± 0.0130	15.1067 ± 0.0135	− 0.0332 ± 0.0233	0.0374 ± 0.0187
FE08	14.9361 ± 0.0187	14.9336 ± 0.0142	14.9455 ± 0.0124	− 0.0025 ± 0.0235	0.0119 ± 0.0188
FE09		22.6983 ± 0.0154	22.7332 ± 0.0126		0.0349 ± 0.0199
FE13	− 2.9319 ± 0.0273	− 2.937 ± 0.0197		− 0.0051 ± 0.0337	
SN03		44.5153 ± 0.0092			
SN04		− 5.3797 ± 0.0116			
SN06		8.9596 ± 0.0091			
SN09		33.1905 ± 0.0115	33.2105 ± 0.0119		0.0200 ± 0.0165
SN11		− 12.5062 ± 0.0090	− 12.5008 ± 0.0116		0.0054 ± 0.0147
SN12		0 ± 0.0000	0 ± 0.0000		0 ± 0.0000
SN14		− 6.1528 ± 0.0114	− 6.1915 ± 0.0137		− 0.0387 ± 0.0178
SN15		34.3430 ± 0.0135	34.2937 ± 0.0101		− 0.0493 ± 0.0169
SN21		34.6705 ± 0.0098	34.6606 ± 0.0084		− 0.0099 ± 0.0129
SN24		35.2319 ± 0.0121	35.2249 ± 0.0123		− 0.0070 ± 0.0172
SN25		37.1955 ± 0.0156			
SN26		30.9968 ± 0.0159	30.9851 ± 0.0253		− 0.0117 ± 0.0299

5.3. Gravity observations

Table 2 presents reduced gravity values and error estimates for annual campaigns at Sierra Negra and Fernandina. Gravity changes at Sierra Negra between 2001 and 2002 were corrected for the effect of vertical displacement of the observation site within the Earth's gravity gradient (− 0.3086 μGal/mm) and are plotted as a function of height change in Fig. 9. Recall that in 2001–2002, meager displacements and relatively large estimated errors in the gravity observations conspire to make any conclusions very uncertain. In general, we can conclude that, on average, sites within the caldera showed decreases in free-air corrected (residual) gravity and subsidence. Changes at SN15, which lies outside the caldera area, are anomalous and so will be omitted in the analysis that follows. The relation between residual gravity change and subsidence at the seven remaining stations is +0.197 μGal/mm.

Gravity changes at Fernandina have large relative uncertainties, owing to the very small displacements at Fernandina over the course of this study. The gravity measurements will serve as a robust baseline for future work, especially if Fernandina continues to inflate or it erupts, but the measurements do not constrain strongly the source of the 2000–2002 deformation there.
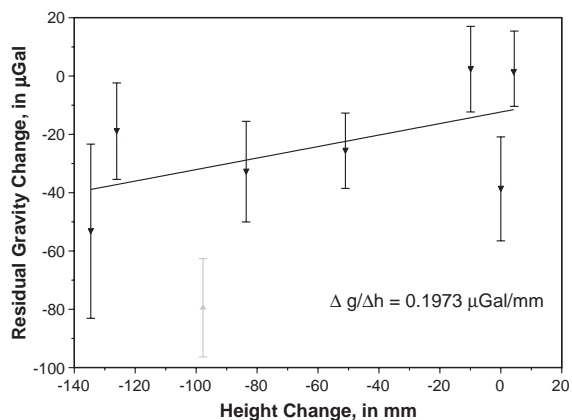

Fig. 9. Residual gravity changes (after correction for free-air effect) at Sierra Negra plotted against observed height change for 2001–2002. Gravity changes and height changes are relative to SN12. Changes at SN15 (grey) are anomalous and are not analyzed here. A fit to the relation between residual gravity and height change (0.197 μGal/mm) is plotted on the figure.

6. Discussion

6.1. Sierra Negra

Our GPS monitoring network documented a fundamental shift in behavior at Sierra Negra. After a decade of high inflation rates in the caldera, the volcano changed to a pattern of deflation. This transition probably occurred sometime in 2000 or 2001. The rate of subsidence observed in 2001–2002 (~9 cm/a) is over 6 times less than the maximum uplift rate (~60 cm/a) observed by InSAR in 1998–1999 (Amelung et al., 2000).

Similar changes from inflation to deflation and back again *without eruption* have been observed at other mafic volcanoes. For example, alternating episodes of inflation and deflation have been documented since 1966 at Askja volcano, Iceland, and are attributed to pressure changes in a shallow magma reservoir (Tryggvason, 1989; Rymer and Tryggvason, 1993; Camitz et al., 1995). Likewise, pronounced subsidence events during longer-term inflationary trends at Kilauea volcano, Hawaii, have been interpreted as due to magma withdrawal from shallow sill-like magma reservoirs beneath the summit caldera (Ryan et al., 1983). Similarly, Mauna Loa volcano, Hawaii, started inflating immediately after its 1984 eruption, but by 1994 it had begun to subside (Miklius et al., 1995). Then, in May 2002, the deflation abruptly changed back to inflation (Miklius et al., 2002). Another example is Medicine Lake volcano, California, where subsidence has been occurring at a rate of about 1 cm/a since 1954 (Dzurisin et al., 1991, 2002). Dzurisin et al. (2002) rule out magma withdrawal, thermal contraction, or crystallization as causal mechanisms at Medicine Lake and instead call upon gravitational loading and tectonic extension. They also note that in the long-term steady subsidence and episodic uplifts caused by magma intrusion probably alternate and counteract each other.

At subduction-zone volcanoes, deflation without eruption has been attributed to fluid loss or reduced pore-fluid pressure within shallow hydrothermal systems at Kiska volcano, Alaska (Lu et al., 2002), Kuju volcano, Japan (Nakaboh et al., 2003). and Cerro Blanco volcano, Argentina (Pritchard and Simons, 2004). At Taal volcano, Philippines, alternating periods of inflation and deflation occurred between 1998 and 2001 and were attributed to episodes of magma intrusion followed by exsolution of magmatic volatiles into an overlying hydrothermal system (Bartel et al., 2003).

Several silicic calderas have also demonstrated similar behavior, with shifts from inflation to deflation unaccompanied by eruption. The most notable examples are Campi Flegri (Barberi and Carapezza, 1996), Long Valley (Battaglia et al., 1999, 2003a,b), and Yellowstone (Dzurisin et al., 1994, 1999). The inflection has usually been attributed to perturbations in their hydrothermal systems (De Natale and Pingue, 1996), although viscoelastic relaxation of the outer boundary of a magma chamber has also been called upon at Long Valley and Campi Flegri (Barberi and Carapezza, 1996; Newman et al., 2001, 2005).

At Sierra Negra, magma movement is the most obvious explanation for the change from uplift to subsidence. The lateral intrusion of magma out of the shallow, subcaldera reservoir would have likely caused major movements of the GPS stations around the caldera rim and on the flanks, but no such displacements were observed, thus we do not favor that hypothesis. Also, any rapid intrusion would also have generated earthquakes, but no significant seismicity was detected either by local land-based seismometers (Minard Hall and Doug Toomey, personal communication, 2004) or by regional hydrophone arrays (Fox et al., 2001; Robert Dziak, personal communication, 2004).

In 2000–2001, the center of the caldera uplifted, but the northern and southern margins deflated (Fig. 4). The simultaneous inflation and deflation cannot be modeled with a single pressure source. We speculate that two magma bodies may have conspired to produce this pattern: a deeper body deflating produced a broad subsidence, while a shallower body inflates to produce a sharper zone of uplift. A quantitative model is underconstrained, however, given the sparse data in 2000–2001 and the measurement uncertainties.

Two simple elastic deformation models are examined to model the 2001–2002 velocities, by least-squares inversion of point and sill-shaped dislocation sources using the program DisModel, developed by P. Cervelli and J. Murray (Cervelli et al., 2002). The point-source model inversion locates the source between stations SN09 and SN26 near the center of the caldera at a depth of 2.3 km and has a mean

standard error (MSE) of 11.7. The volume change required to account for the subsidence is a decrease of 2.6 million m^3. The worst fitting stations for this model are SN27 and SN08, both of which show displacements that are directed more westerly than point source model displacements.

An expanding sill model best fits the 1992-1998 uplift seen by InSAR (Amelung et al., 2000), and a number of pieces of evidence suggest that the uppermost parts of the subcaldera plumbing systems consist of thin sills in the western Galápagos (Geist and Teasdale, 2001). The best-fitting dislocation source for the subsidence at Sierra Negra is a sill whose horizontal dimensions are 5.3×3.0 km and whose depth is 2.1 km (Fig. 10). The coordinates of the center of the sill are 91.125° W, 0.830° S, and the long axis strikes N66E. It is notable that this geometry essentially outlines the prominent sinuous fault system on the western caldera floor, which has previously been attributed to upheaval by shallow intrusion (Reynolds et al., 1995; Amelung et al., 2000). The best fit source indicates subsidence of the roof of the sill by 26 cm, amounting to 4.1 million m^3 of volumetric contraction. This sill model largely corrects the misfit that SN08 and SN27 have with the point source model, and has an MSE of 7.1. This sill model is similar to that derived by Amelung et al. (2000) for

the 1998–1999 InSAR results, although their model was more sophisticated and involved a sill that tapers towards its edges. The part of their sill with significant opening (>30 cm) almost exactly matches the dimensions and location of the sill modeled here. Remarkably, the subsidence detected by GPS in 2001–2002 at Sierra Negra, roughly cancelled out the uplift documented by InSAR and GPS in 1998–2000.

We attribute the 2000–2001 inflation at Sierra Negra to a waning continuation of the inflation measured by Amelung et al. (2000), caused by shallow intrusion of magma beneath the caldera. No other feasible process could result in nearly 3 m of uplift over less than a decade. The 2001–2002 deflation on the other hand could be due to a number of processes, however. Once intrusion halted, vesiculated magma within the shallow magma reservoir may have degassed by segregation of the vesicles from the magma. Sierra Negra has a very active hydrothermal system that contains a large component of magmatic gas (Goff et al., 2000). The hydrothermal system is not monitored, however, and we have not noticed any obvious change in the fumaroles in six visits since 1983 by Geist. Alternatively, some of the magma that had entered the shallow magma body beneath the caldera (and was responsible for the inflation) may have withdrawn back down the magmatic plumbing
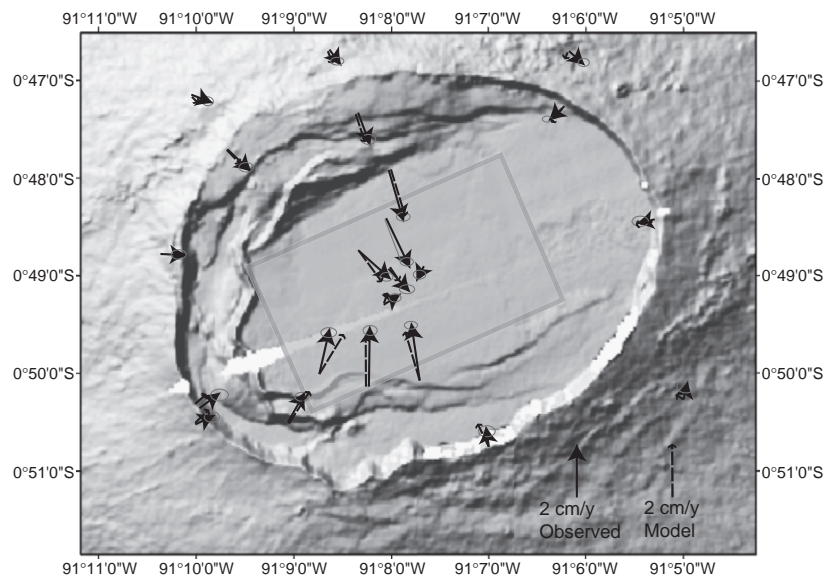

Fig. 10. Illustration of the best-fitting horizontal sill to explain 2001–2002 deflation of Sierra Negra's caldera.

system in 2001. The decrease in driving pressure required for such an event could be caused by normal faulting at depth, deep lateral flow of magma, or outward flow of ultramafic or mafic cumulates (Clague and Denlinger, 1994). Finally, the transition from inflation to deflation may coincide with a change from elastic behavior of the surrounding rocks during intrusion followed by viscous flow of the rocks outward after intrusion has lulled (Newman et al., 2001).

The approximately 3-yr interval between the trap-door fault episode on the southern caldera floor and the transition from inflation to deflation may be significant. For example, the sudden uplift may have lowered the confining pressure on the shallow sill, which then triggered a degassing episode, or the stress change may have upset the plumbing system between the shallow reservoir and the deeper system that supplies it.

In the absence of a dense seismic network, differentiating between degassing, viscous flow, and downward intrusion are best discerned through a combination of gas monitoring and precise gravity monitoring. In the event of degassing, subsurface volume is lost with essentially no loss of mass. In the event of intrusive drainback or viscous flow, both mass and volume are moved away from the surface, resulting in a significant change in gravity. Analysis of the gravity observations made in 2001–2002 support the interpretation that the subsidence was due to removal of magma mass and not simply a volume reduction that would accompany densification by degassing or cooling contraction. For a sill-shaped deformation source, the ratio of free-air corrected gravity residuals to height change is expected to be near 0.109 μGal/mm if the density of the injected mass is 2600 kg/m^3 (Savage, 1984). Ratios less than 0.109 μGal/mm imply that the density of the mass removed to generate the subsidence is less than 2600 kg/m^3 or that some of the subsidence was due to subsurface density increase (Johnson, 1992, 1995). Conversely, ratios greater than 0.109 μGal/mm suggest that higher density mass was removed from the subsurface reservoir or that subsurface densities decreased. Because the observed ratio is slightly larger than 0.109 μGal/mm (Fig. 9), mechanisms that include mass loss and density decreases are favored. Movement of magma (mass) out of the reservoir, either laterally away from the monitoring network or

downward, is the most likely possibility. In situ contraction by cooling or degassing of the magma chamber as a cause of the subsidence is not supported by the gravity observations.

6.2. Fernandina

The deformation pattern observed at Fernandina is vastly simpler than that at Sierra Negra, perhaps in part because there are no data from the caldera floor. The pattern at Fernandina is a fairly simple, steady, radial-outward motion typical of a shallow inflationary source. Because the pattern of deformation in the two intervals 2000–2001 and 2001–2002 are similar, we focus on the latter, because of the larger data set.

The best-fitting point source model for expansion of the summit region (MSE=6.8) during 2001–2002 is located at 91.54° W, 0.37° S at a depth of only 1.0 km, with a volume expansion of 500,000 m^3. A 3×3 km sill source centered beneath the caldera fits equally well (MSE=5.7), with 37 cm of upward expansion at 2.1 km depth, amounting to a volume increase of 1.2 million m^3.

Fernandina is apparently in a period of slow inflation between eruptions. It is the most active volcano in Galápagos; during the last five decades it has erupted every few years (1958, 1961, 1968, 1972, 1973, 1977, 1978, 1981, 1984, 1988, 1991, 1995; Simkin and Siebert, 1994). Twenty million m^3 of lava were erupted during the 1995 eruption (Rowland, 1996). At the current rate of inflation, it would take 20 to 30 yrs to recharge the magma reservoir to its volume before 1995, assuming 25% vesicularity in the 1995 flow. This suggests that the rate of inflation at Fernandina is not constant, and it probably varies significantly over time, e.g. the inflation rate would have had to be significantly higher during most of the 1990s to account for the frequent eruptions. On the other hand, we note that there was an hiatus of over 20 yrs between 1937 and 1958 when no eruptions were observed (Simkin and Siebert, 1994), also suggesting a variable magma supply rate.

The absence of lateral motions along the coast of Fernandina indicates that steady flank slip is not currently an important process in the growth of this volcano (Fig. 8), despite that steep submarine slopes cascade to depths of >3 km to the north and west of the volcano. This is consistent with the lack of large

landslide deposits on the deep sea floor around Fernandina (Fornari et al., 2001). Thus, although prodigious landslides are prevalent around Reunion and the Hawaiian and Canary Islands (Duffield et al., 1982; Holcomb and Searle, 1991; Moore et al., 1994; Marti et al., 1997), they are apparently not a ubiquitous feature of all ocean islands.

Gravity observations at Fernandina are (Table 2) are inconclusive. Changes observed in 2000–2001 were not repeated in 2001–2002, which suggests that meaningful variations were not detected. Certainly, the Fernandina gravity observations provide an excellent baseline in the event that the volcanic and deformational activity increases.

7. Conclusions

GPS and microgravity measurements on active volcanoes in the Galápagos indicate that deformation is caused by the movement of magma at very shallow levels beneath the caldera floor. The rates of deformation are especially irregular at Sierra Negra and punctuated by trapdoor faulting and episodes of deflation unaccompanied by eruption. Our best estimates for the tops of the shallow magma chambers beneath Fernandina and Sierra Negra calderas are between 1 and 2 km, which puts them at very near sea level. That large volumes of magma accumulate at such shallow levels without erupting is truly remarkable. At Sierra Negra, after a decade of rapid uplift, the caldera abruptly began to subside in late 2000 or early 2001 (Figs. 11 and 12). Mea-

Fig. 12. The rate of uplift of the center of the caldera of Sierra Negra with time. Measurements before 2000 are from Amelung et al. (2000) and measured by InSAR.

surements by a continuously monitored single frequency GPS network since May, 2002 has revealed that Sierra Negra renewed inflating in 2003, and the rate of inflation has accelerated to ~67 cm/a at the time of this writing (December, 2004; Geist et al., 2004 and unpublished data). Despite such a dynamic magmatic system, there has been no eruption at Sierra Negra since 1979. It seems unlikely that such large rates of intrusion can continue for very long without eruption, even with trapdoor faulting (Amelung et al., 2000) relieving the pressure exerted by the newly intruded magma. Continued monitoring until the next eruption will enable us to ascertain the feedback between intrusion, eruption, and surface deformation.

At Fernandina, inflation rates are currently more modest and steady, although we do not know how the caldera floor is behaving. The lower rates of inflation here are somewhat surprising, because this is the most active volcano in the archipelago, although it is conceivable that the 1995 eruption was unusually voluminous, and recharge may take longer than has been typical for the past half-century. Continued deformation monitoring will constrain the rate of magma recharge between eruptions.

According to our measurements, the flanks of these volcanoes are stable, in stark contrast with the mobile flanks of active Hawaiian volcanoes. This observation validates the hypothesis of Nakamura (1980), who suggested that flank instability may depend on the age of the underlying ocean crust. Where the crust is old (like in Hawaii or the Canary Islands) the existence of thick sediments allows the volcano flanks to slip, whereas where the ocean crust is young (like
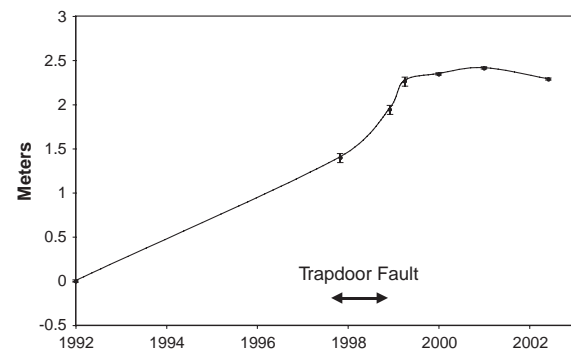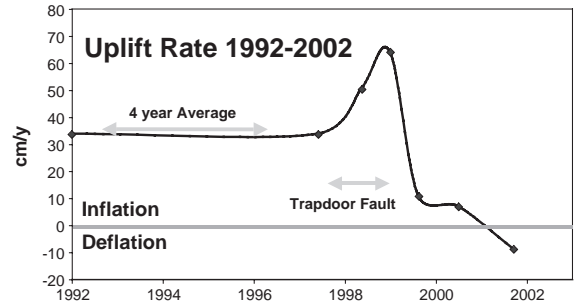

Fig. 11. The vertical path of the center floor of the caldera of Sierra Negra with time. Measurements before 2000 are from Amelung et al. (2000) and measured by InSAR.

in the Galápagos) the flanks do not slip. Another contributing factor is that the Galápagos volcanoes are not buttressed by their nearest neighbor, as are their Hawaiian counterparts; instead of growing sequentially on the flanks of the next-youngest volcano, the western Galápagos shields have emerged and grown essentially simultaneously (Naumann and Geist, 2000).

Previous hypotheses for the unusual morphologies of the western Galápagos shields include permanent deformation (uplift) by shallow sills (Cullen et al., 1987) or cone sheets (Nordlie, 1973). Although the data presented here shows that the Galápagos volcanoes deform both elastically and by faulting (Amelung et al., 2000), the deformation we have observed has been mostly restricted to the calderas.

Deformation of volcanoes is known to be highly variable in both magnitude and direction, over time scales ranging from a few days to a few years; this transient behavior has particularly been born out by continuous GPS monitoring (e.g. Battaglia et al., 1999; Newman et al., 2001, 2005; Bartel et al., 2003) and calls into question the usefulness of periodic sampling with a campaign strategy. Our having missed the details of the transition from inflation to deflation in 2000–2001 exemplifies this point. Moreover, the continuous network that has been monitoring Sierra Negra since May, 2002 reveals at least five episodes of change in deformation rate through September, 2004, including a transition from deflation to inflation (Geist et al., 2004); this not only would have been missed by an annual campaign, no motion would be measured despite nearly 10 cm of subsidence followed by 10 cm of uplift. In any event, new GPS deformation monitoring networks are now in place at the two most active Galápagos shield volcanoes. Therefore, we are now poised to learn more from future eruptions at these very active volcanoes.

Acknowledgements

References

Amelung, F., Jonsson, S., Zebker, H., Segall, P., 2000. Widespread uplift and "trapdoor" faulting on Galápagos volcanoes observed with radar interferometry. Nature 407, 993–998.

Banfield, A.F., BehreJ Jr., C.H., St. Clair, D., 1956. Geology of Isabela (Albemarle) Island, Archipelago de Colon (Galápagos). Geol. Soc. Am. Bull. 67, 215–234.

Barberi, F., Carapezza, M.L., 1996. The problem of volcanic unrest; the Campi Flegrei case history. In: Scarpa, R., Tilling, R. (Eds.), Monitoring and Mitigation of Volcano Hazards. Springer-Verlag, Berlin.

Battaglia, M., Roberts, C., Segall, P., 1999. Magma intrusion beneath Long Valley Caldera confirmed by temporal changes in gravity. Science 285, 2119–2122.

Battaglia, M., Segall, P., Murray, J., Cervelli, P., Langbein, J., 2003. The mechanics of unrest at Long Valley caldera, California: 1. Modeling the geometry of the source using GPS, leveling and two-color EDM data. J. Volcanol. Geotherm. Res. 127, 195–217.

Battaglia, M., Segall, P., Roberts, C., 2003. The mechanics of unrest at Long Valley caldera, California: 2. Constraining the nature of the source using geodetic and micro-gravity data. J. Volcanol. Geotherm. Res. 127, 219–245.

Bartel, B.A., Hamburger, M.W., Meertens, C.M., Lowry, A.R., Corpuz, E., 2003. Dynamics of active magmatic and hydrothermal systems at Taal volcano, Philippines, from continuous GPS measurements. J. Geophys. Res. 108, 2475.

Cervelli, P., Segall, P., Amelung, F., Garbeil, H., Meertens, C., Owen, S., Miklius, A., Lisowski, M., 2002. The 12 September 1999 upper East Rift Zone dike intrusion at Kilauea Volcano, Hawaii. J. Geophys. Res. 107, 2150.

Camitz, J., Sigmundsson, F., Foulger, G., Jahn, C.H., Voelksen, C., Einarsson, P., 1995. Plate boundary deformation and continuing deflation of the Askja volcano, North Iceland, determined with GPS, 1987–1993. Bull. Volcanol. 57, 136–145.

Chadwick, W.W., Dieterich, J.H., 1995. Mechanical modeling of circumferential and radial dike intrusion on Galápagos volcanoes. J. Volcanol. Geotherm. Res. 66, 37–52.

Chadwick, W.W., Howard, K.A., 1991. The pattern of circumferential and radial eruptive fissures on the volcanoes of Fernandina and Isabela islands, Galápagos. Bull. Volcanol. 53, 259–275.

Chadwick Jr., W.W., De Roy, T., Carrasco, A., 1991. The September 1988 intracaldera avalanche and eruption at Fernandina volcano, Galápagos Islands. Bull. Volcanol. 53, 276–286.

Clague, D., Denlinger, R.P., 1994. Role of olivine cumulates in destabilizing the flanks of Hawaiian volcanoes. Bull. Volcanol. 56, 425–434.

Cullen, A.B., McBirney, A.R., Rogers, R.D., 1987. Structural controls on the morphology of Galápagos shields. J. Volcanol. Geotherm. Res. 34, 143–151.

De Natale, G., Pingue, F., 1996. Ground deformation modeling in volcanic areas. In: Scarpa, R., Tilling, R. (Eds.), Monitoring and Mitigation of Volcano Hazards. Springer-Verlag, Berlin.

Dieterich, J.H., 1988. Growth and persistence of Hawaiian volcanic rift zones. J. Geophys. Res. 93, 4258–4270.

Duffield, W.A., Stieltjes, L., Varet, J., 1982. Huge landslide blocks in the growth of Piton de la Fournaise, La Reunion, and Kilauea Volcano, Hawaii. J. Volcanol. Geotherm. Res. 12, 147–160.

Dvorak, J.J., Dzurisin, D., 1997. Volcano geodesy: the search for magma reservoirs and the formation of eruptive vents. Rev. Geophys. 35, 343–384.

Dzurisin, D., Donnelly-Nolan, J.M., Evans, J.R., Walter, S.R., 1991. Crustal subsidence, seismicity, and structure near Medicine Lake volcano, California. J. Geophys. Res. 96, 16319–16333.

Dzurisin, D., Yamashita, K.M., Kleinman, J.W., 1994. Mechanism of crustal uplift and subsidence at the Yellowstone caldera, Wyoming. Bull. Volcanol. 56, 261–270.

Dzurisin, D., Wicks Jr., C., Thatcher, W., 1999. Renewed uplift at the Yellowstone Caldera measured by leveling surveys and satellite radar interferometry. Bull. Volcanol. 61, 349–355.

Dzurisin, D., Poland, M.P., Bürgmann, R., 2002. Steady subsidence of Medicine Lake volcano, northern California, revealed by repeated leveling surveys. J. Geophys. Res. 107, 2372.

Fornari, D.J., Kurz, M.D., Geist, D.J., Johnson, P.D., Peckman, U.G., Scheirer, D., 2001. New perspectives on the structure and morphology of the submarine flanks of Galápagos Volcanoes—Fernandina and Isabela. Eos Trans. AGU 82 (Fall Meet. Suppl.)

Fox, C.G., Matsumoto, H., T.-K.A.,, 2001. Monitoring Pacific Ocean seismicity from an autonomous hydrophone array. J. Geophys. Res. 106, 4183–4206.

Freymueller, J.T., Kellogg, J.N., Vega, V., 1993. Plate motions in the North Andean region. J. Geophys. Res. 98, 21853–21863.

Geist, D.J., Howard, K.A., Jellinek, A.M., Rayder, S., 1994. Volcanic history of Volcán Alcedo, Galápagos Archipelago: a case study of rhyolitic oceanic volcanism. Bull. Volcanol. 56, 243–260.

Geist, D., White, W.M., Albarede, F., Harpp, K.S., Blichert-Toft, J., Reynolds, R., Kurz, M., 2002. Volcanic evolution in the Galápagos: the dissected shield of Volcan Ecuador. Geochem. Geophys. Geosyst. 3 (10) (10611,1029/2002GC000355).

Geist, D., Teasdale, R., 2001. Lithospheric evolution of Galápagos magmas. Eos Trans. AGU 82 (47) (Fall Meet. Suppl., Abstract T41D-05).

Geist, D., Naumann, T., Standish, J., Harpp, K., Kurz, M., Fornari, D., 2003. Diffuse rift zones: subaerial and submarine satellite vents at Wolf volcano, Galápagos. Eos Trans. AGU 84 (46) (Fall Meet. Suppl., Abstract V12G-04).

Geist, D., Johnson, D., Chadwick, W., Meertens, C., Feaux, K., 2004. Cyclical inflation and deflation at Sierra Negra Volcano, Galapagos revealed by continuous single-frequency GPS Monitoring. Eos Trans. AGU 85 (17) (Jt. Assem. Suppl., Abstract V53B-01).

Goff, F., McMurtry, G.M., Counce, D., Simac, J.A., Roldan-Manzo, A.R., Hilton, D.R., 2000. Contrasting hydrothermal activity at Sierra Negra and Alcedo volcanoes, Galápagos Archipelago, Ecuador. Bull. Volcanol. 62, 34–52.

Holcomb, R.T., Searle, R.C., 1991. Large landslides from oceanic volcanoes. Mar. Geotechnol. 10, 19–32.

Hugentobler, U, Schaer, S, Fridez, P (Eds.), 2001. Bernese GPS Software Version 4.2, Astron. Inst. Univ. of Berne, Berne, Switzerland, 515 pp.

Johnson, D.J., 1992. Dynamics of magma storage in the summit reservoir of Kilauea Volcano, Hawaii. J. Geophys. Res. 97, 1807–1820.

Johnson, D.J., 1995. Gravity changes on Mauna Loa Volcano. In: Rhodes, J.M., Lockwood, J.P. (Eds.), Mauna Loa Revealed: Structure, Composition, History and Hazards, Geophysical Monograph, vol. 92. AGU, Washington, D.C., pp. 127–144.

Jonsson, S., Zebker, H., Cervelli, P., Segall, P., Garbeil, H., Mouginis-Mark, P., Rowland, S.A., 1999. Shallow-dipping dike fed the 1995 flank eruption at Fernandina Volcano, Galápagos, observed by satellite radar interferometry. Geophys. Res. Lett. 26, 1077–1080.

Lénat, J.F., Vincent, P., Bachèlery, P., 1989. The off-shore continuation of an active basaltic volcano: Piton de la Fournaise (Reunion Island, Indian Ocean); structural and geomorphological interpretation from Sea Beam mapping. J. Volcanol. Geotherm. Res. 36, 1–36.

Lipman, P.W., 1997. Subsidence of ash-flow calderas; relation to caldera size and magma-chamber geometry. Bull. Volcanol. 59, 198–218.

Lu, Z., Masterlark, T., Power, J., Dzurisin, D., Wicks Jr., C., 2002. Subsidence at Kiska volcano, Western Aleutians, detected by satellite radar interferometry. Geophys. Res. Lett. 29, 1855.

Marti, J., Hurlimann, M., Ablay, G.J., Gudmundsson, A., 1997. Vertical and lateral collapses on Tenerife (Canary Islands) and other volcanic ocean islands. Geology 25, 879–882.

McBirney, A.R., Williams, H., 1969. Geology and petrology of the Galápagos Islands. Geolog. Soc. Amer. Mem. 118 (197 pp.).

Miklius, A., Cervelli, P., Lisowski, M., Sako, M., Koyanagi, S., 2002. Renewed inflation of Mauna Loa volcano, Hawaii. Eos Transact. Amer. Geophys. Union 83 (47, Fall Meet. Suppl.) (Abstract T12A-1290).

Miklius, A., Cervelli, P., Lisowski, M., Sako, M., Koyanagi, S., 1995. Recent inflation and flank movement of Mauna Loa Volcano. In: Rhodes, J.M., Lockwood, J.P. (Eds.), Mauna Loa

Revealed: Structure, Composition, History and Hazards. American Geophysical Union, Washington, DC, pp. 199–205.

Moore, J.G., Normark, W.R., Holcomb, R.T., 1994. Giant Hawaiian landslides. Ann. Rev. Earth. Planet. Sci. 22, 119–144.

Nakaboh, M., Ono, H., Sako, M., Sudo, Y., Hashimoto, T., Hurst, A.W., 2003. Continuing deflation by fumaroles at Kuju volcano, Japan. Geophys. Res. Lett. 30, 1396.

Nakamura, K., 1980. Why do long rift zones develop in Hawaiian volcanoes—a possible role of thick oceanic sediments. Bull. Volcanol. Soc. Japan 25, 255–267 (in Japanese).

Naumann, T., Geist, D., 2000. Physical volcanology and structural development of Cerro Azul volcano, Isabela island, Galápagos: implications for the development of Galápagos-type shield volcanoes. Bull. Volcanol. 61, 497–514.

Newman, A.V., Dixon, T.H., Ofoegbu, G.I., Dixon, J.E., 2001. Geodetic and seismic constraints on recent activity at Long Valley Caldera, California: evidence for viscoelastic rheology. J. Volcanol. Geotherm. Res. 105, 183–206.

Newman, A.V., Dixon, T.H., Gourmelen, N., 2005. A four-dimensional viscoelastic deformation model for Long Valley Caldera, California, between 1995 and 2000. J. Volcanol. Geotherm. Res. 150, 244–269 (this volume).

Nordlie, B.E., 1973. Geology and structure of the western Galápagos volcanoes and a model for their origin. Geol. Soc. Amer. Bull. 84, 2931–2956.

Owen, S., Segall, P., Freymueller, J., Miklius, A., Denlinger, R., Arnadottir, T., Sako, M., Burgmann, R., 1995. Rapid deformation of the south flank of Kilauea volcano, Hawaii. Science 267, 1328–1332.

Poland, M.P., 2001. Determining the stress regime within a volcanic edifice from igneous intrusions and deformation measurements. PhD thesis, Arizona State University.

Pritchard, M.E., Simons, M., 2004. An InSAR-based survey of volcanic deformation in the central Andes. Geochem. Geophys. Geosys. 5 (2) (Q02002).

Reynolds, R., Geist, D., Kurz, M., 1995. Physical volcanology and structural development of Sierra Negra volcano, Galápagos Archipelago. Geol. Soc. Amer. Bull. 107, 1398–1410.

Rowland, S.K., 1996. Slopes, lava flow volumes, and vent distributions on Volcán Fernandina, Galápagos Islands. J. Geophys. Res. 101, 27657–27673.

Rowland, S.K., Munro, D.C., 1992. The caldera of Volcan Fernandina: a remote sensing study of its structure and recent activity. Bull. Volcanol. 55, 97–109.

Ryan, M.P., Blevins, J.Y.K., Okamura, A.T., Koyanagi, R.Y., 1983. Magma reservoir subsidence mechanics: theoretical summary and application to Kilauea volcano, Hawaii. J. Geophys. Res. 88, 4147–4181.

Rymer, H., Tryggvason, E., 1993. Gravity and elevation changes at Askja, Iceland. Bull. Volcanol. 55, 362–371.

Savage, J.C., 1984. Local gravity anomalies produced by dislocation sources. J. Geophys. Res. 89, 1945–1952.

Simkin, T., 1984. Geology of Galápagos Islands. In: Perry, R. (Ed.), Galápagos. Pergamon Press, Oxford, pp. 15–41.

Simkin, T., Howard, K.A., 1970. Caldera collapse in the Galápagos islands. Science 169, 429–437.

Simkin, T., Siebert, L., 1994. Volcanoes of the World, 2nd ed. Geoscience Press, Tucson, AZ. 349 pp.

Swanson, D.A., Duffield, W.A., Fiske, R.S., 1976. Displacement of the south flank of Kilauea Volcano: the result of forceful intrusion of magma into the rift zones. U. S. Geol. Surv. Prof. Pap. 963 (39 pp.).

Tryggvason, E., 1989. Ground deformation in Askja, Iceland: its source and possible relation to flow of the mantle plume. J. Volcanol. Geotherm. Res. 39, 61–71.

Walker, G.P.L., 1988. Three Hawaiian calderas: an origin through loading by shallow intrusions? J. Geophys. Res. 93, 14773–14784.

Williams, H., McBirney, A.R., 1979. Volcanology. Freeman Cooper, San Francisco, p. 397.

Wilson, R.M., 1935. Ground Surface Movement at Kilauea Volcano, Hawaii, vol. 10. Hawaii University Research Publication. 56 pp.

Wood, C., 1984. Calderas: a planetary perspective. J. Geophys. Res. 89, 8391–8406.